Electronic Supplementary Material

1. Materials

Fluorine-doped tin oxide (FTO) - coated glass (14 Ω/cm^2) with an area of 1.5 cm ×3 cm, 0.015 M acetylacetone (Sigma-Aldrich), 0.05 M tetrabutyl titanate (Sigma-Aldrich), 0.05 M anhydrous ethanol, deionized water (18.2 MΩ·cm@25°C), HCl (Sigma-Aldrich), $Bi(NO_3)_3·5H_2O$ (Sinopharm Chemical Reagent, 99.99%), vanadium (IV)-oxy acetylacetonate (Macklin, 99%), DMSO (Sinopharm Chemical Reagent, AR), 0.5 M Na_2SO_4 (Sinopharm Chemical Reagent, AR).

2. Experimental procedures

2.1 Preparation of TiO_2 seed layer

0.015 M acetylacetone, 0.05 M tetrabutyl titanate, and 0.05 M anhydrous ethanol were dissolved in 50 mL of deionized water and stirred for 1 h to form a milky suspension. FTO with an area of 1.5 cm ×3 cm was used as substrate, which was sonicated in acetone, deionized water, and anhydrous ethanol sonicated for 15 min in sequence. The milky suspension was spin-coated onto FTO substrates at 1200 r/min for 60 s, followed by heating in air at 60 °C for 15 min. The spin-coating process was repeated 3 times for each sample, and the samples were then annealed in a muffle furnace at 450° C for 30 min at a heating rate of 5 °C/min.

2.2 Preparation of TiO_2 nanorods

FTO substrates with seed layers were placed in the Teflon liner with the conductive surface facing down, filled with 63 mL of aqueous solution containing 0.05 M tetrabutyl titanate and 33 mL of HCl. The kettle was sealed and placed in an autoclave at 160 °C for 6 h. After the hydrothermal process, the samples were taken out and rinsed with deionized water, dried on a hot plate at 60 °C, and further annealed in a muffle furnace at 450 °C for 2 h in air [1].

2.3 Preparation of $BiVO_4$ nanorods

The synthetic procedure for the worm-like $BiVO_4$ were modified from that reported by Zhang and co-workers [2]. The precursor solution were prepared by dissolving 0.6 M $Bi(NO_3)_3·5H_2O$ and an excessive concentrations of $VO(acac)_2$ (6%) in DMSO solution. Then, the precursor solution was filtered by 0.22 μm filtration membrane for use. The precursor films were prepared by a spin-coating process on FTO glass substrate, followed by the pyrolysis process. Specifically, a 100 μL precursor solution was dropping onto the clean FTO of 1.5 cm ×3 cm, with a spin-coating speed of 1000 r/min for 10 s and 3000 r/min for 30 s, then the FTO was heated on the hot plate at 130 ℃ for 30 minutes. This process was repeated 6 times for best performance. Then, the $BiVO_4$ films were annealed in a muffle furnace at 450 ℃ and for 2 hours.

2.4 Preparation of TiO_2/$BiVO_4$ nanorods

For the preparation of TiO_2/$BiVO_4$ photoanode, the substrate was replaced by TiO_2 photoanode. Subsequent operations are the same as those of the worm-like $BiVO_4$ photoanode.

3. Characterization

Scanning electron microscopy (SEM, JSM-7800F, JEOL, Japan) was used to characterize the morphology and the microstructure of samples on FTO substrates. The parameters for SEM were 3 kV, 8 mA probe current, and a 6 mm working distance. X-ray diffraction (XRD, Panalytical) with Cu Kα radiations, 40 kV, 40 mA was applied to identify the crystal structure and phase for the samples. The

ultraviolet-visible absorption spectra from 300 to 800 nm were taken on a spectrophotometer (UV-Vis, Cary-5000, Agilent Technologies, Inc).

4. Photoelectrochemical performance

Photoelectrochemical (PEC) performance of all prepared samples and PV cells were tested with a fiber optic light source (PLS-FX300HU, Beijing Perfect Light Technology Co., Ltd., Beijing, China) with an air mass 1.5 global (AM 1.5G) filter. The light intensity was carefully calibrated to ca. 1000 W m^{-2} by a light power meter (PL-MW2000, Beijing Perfect Light Technology Co., Ltd., Beijing, China). A platinum electrode (1×1 cm) and an Ag/AgCl (3 M KCl) electrode were used as the counter electrode and reference electrode, respectively. The electrolyte solution was 0.5 M Na_2SO_4 solution. Photocurrent-potential curves were obtained with a scan rate of 10 mV s^{-1} on an electrochemical workstation (CHI 760D).

All the potentials versus RHE were converted according to the Nernst equation:

$$E_{\mathrm{RHE}} = E_{\frac{\mathrm{Ag}}{\mathrm{AgCl}}} + 0.059 * pH + E^{0}_{\frac{\mathrm{Ag}}{\mathrm{AgCl}}}, \quad \text{(S1)}$$

where E_{RHE} refers to the converted potential versus RHE. The value of $E^{0}_{\frac{\mathrm{Ag}}{\mathrm{AgCl}}}$ is 0.197 V at ambient temperature (25 °C) and $E_{\frac{\mathrm{Ag}}{\mathrm{AgCl}}}$ is the obtained potential versus Ag/AgCl. Applied bias photon-to-current efficiency (ABPE) can be calculated using

$$ABPE = \left[\frac{|J_{\mathrm{ph}}|\times(V_{\mathrm{redox}}-V_{\mathrm{app}})(V)\times\eta_F}{P_{\mathrm{light}}}\right], \quad \text{(S2)}$$

where J_{ph} is the photocurrent density (mA·m^{-2}) obtained from the electrochemical workstation; V_{redox} is the thermodynamic potential of the reaction, which is supposed to be 1.23V; V_{app} refers to the applied bias versus RHE (V); η_{F} is the Faraday efficiency, which is defaulted to 100% in the experiment; and P_{light} is the total light intensity of AM 1.5 G (1000 W·m^{-2}).

Incident-photon-to-current conversion efficiency (IPCE) was obtained using a monochromator (TLS-180, Zolix Instruments Co., Ltd., Beijing, China) coupled with a 150 W Xenon lamp as the simulated light source. The light intensity of the monochrome light was calibrated with a photometer (Model IL1400BL).

$$IPCE(\%) = J_{\mathrm{ph}} \times \frac{1240}{\lambda\times P_{\mathrm{light}}} \times 100\%, \quad \text{(S3)}$$

where λ and P_{light} are the incident light wavelength (nm) and the power density obtained at a specific wavelength (W/m^2·nm^{-1}), respectively.

The energy of the TiO_2/$BiVO_4$ in setup 2 is defined as

$$E_{\mathrm{photoanode}} = A_{\mathrm{photoanode}} \int_{300}^{800} I_{\lambda,\mathrm{TiO2/BiVO4}} Abs_{\mathrm{TiO2/BiVO4}} d\lambda, \quad \text{(S4)}$$

where $A_{\mathrm{photoanode}}$ is the area of the TiO_2/$BiVO_4$ photoanode, and $Abs_{\mathrm{TiO2/BiVO4}}$ is the absorbance of the TiO_2/$BiVO_4$ photoanode.

The efficiency of the TiO_2/$BiVO_4$ photoanode can be written as

$$\eta_{\mathrm{photoanode}} = \frac{E_{\mathrm{photoanode}}}{I_{\mathrm{total}} A_{\mathrm{light}}}. \quad \text{(S5)}$$

The TiO_2/$BiVO_4$ photoanode transmits the other spectrum to the Si cell. Therefore, the energy at the PV module can be stated as

$$E_{Si} = A_{Si} \int_{300}^{800} I_{\lambda,\mathrm{TiO2/BiVO4}} T_{\lambda,\mathrm{TiO2/BiVO4}} d\lambda, \quad \text{(S6)}$$

where $T_{\mathrm{TiO2/BiVO4}}$ is the transmittance of the $TiO_2/BiVO_4$ photoanode.

In this case, the energy efficiency from solar light to PV cell output can be defined as

$$\eta_{Si} = \frac{I_{Si} V_{Si}}{E_{Si}} = \frac{FF \times I_{sc,Si} \times V_{OC,Si}}{E_{Si}}, \quad \text{(S7)}$$

where I_{Si} and V_{Si} are the current and voltage at the maximum power output.

The energy of the TiO_2 in Setup 1 is defined as

$$E_{\mathrm{TiO2}} = A_{\mathrm{TiO2}} \int_{300}^{800} I_{\lambda,\mathrm{TiO2}} Abs_{\lambda,\mathrm{TiO2}} d\lambda, \quad \text{(S8)}$$

where A_{TiO2} is the area of the TiO_2 photoanode, and Abs_{TiO2} is the absorbance of the TiO_2 photoanode.

The energy efficiency from solar light to the TiO_2 photoanode can be written as

$$\eta_{\mathrm{TiO2}} = \frac{E_{\mathrm{TiO2}}}{I_{\mathrm{total}} A_{\mathrm{light}}}. \quad \text{(S9)}$$

The TiO_2 photoanode transmits the higher solar spectrum to the $BiVO_4$ photoanode, and the energy arrived the $BiVO_4$ surface can be calculated as

$$E_{\mathrm{TiO2-BiVO4}} = A_{\mathrm{BiVO4}} \int_{300}^{800} I_{\lambda,\mathrm{TiO2}} T_{\lambda,\mathrm{TiO2}} d\lambda, \quad \text{(S10)}$$

where A_{BiVO4} is the area of the $BiVO_4$ photoanode behind the TiO_2 photoanode, and T_{TiO2} is the transmittance of the TiO_2 photoanode.

There is a small solar spectral range transmitted by the TiO_2, which can be absorbed by the $BiVO_4$. Therefore, the energy at the $BiVO_4$ can be stated as

$$E_{\mathrm{BiVO4}} = A_{\mathrm{BiVO4}} \int_{300}^{800} I_{\lambda,\mathrm{BiVO4}} Abs_{\lambda,\mathrm{BiVO4}} T_{\lambda,\mathrm{TiO2}} d\lambda, \quad \text{(S11)}$$

where Abs_{BiVO4} is the absorbance of the $BiVO_4$ photoanode.

The energy efficiency from solar light to the $BiVO_4$ photoanode behind the TiO_2 photoanode can be written as

$$\eta_{\mathrm{BiVO4}} = \frac{E_{\mathrm{BiVO4}}}{E_{\mathrm{TiO2-BiVO4}}}. \quad \text{(S12)}$$

After the TiO_2 and $BiVO_4$ photoanode transmit higher spectrum to the PV cell, the other energy can be stated as

$$E_{Si} = A_{Si} \int_{300}^{800} I_{\lambda,Si} T_{\lambda,\mathrm{TiO2}} T_{\lambda,\mathrm{BiVO4}} d\lambda, \quad \text{(S13)}$$

where T_{BiVO4} is the transmittance of the $BiVO_4$ photoanode behind the TiO_2 photoanode.

The energy efficiency of the PV cell behind the TiO_2 photoanode and $BiVO_4$ photoanode can be defined as

$$\eta_{Si} = \frac{I_{Si} V_{Si}}{E_{Si}} = \frac{FF \times I_{sc,Si} \times V_{OC,Si}}{E_{Si}}. \quad \text{(S14)}$$

5. Supplementary notes

Note 1: A Sankey diagram was constructed to show the energetic flows through the integrated system and was calculated from UV-Vis spectra. Reasonable estimates were made as outlined in the following paragraph.

The total light power flux and power incident on the system was determined from the solar collection area (i.e., BS area) and the light intensity measured with optical power meter (PL-MW 2000).

As shown in Fig. 8, the energy density of sunlight in the 300–800 nm range is 58.912 mW/cm^2, and the area of solar cell and photoelectrode is 0.25 cm^2. Therefore, the theoretical energy arriving at the system is 14.728 mW. The amount of light reflected or transmitted by the BS was estimated by the reflected or transmitted spectrum of UV-Vis. PV electrical power transferred to the PEC is known through the linear sweep voltammetry method. The outlet light and heat losses from the system were calculated based on the amount of the total light input and the transmission of the BS and photoelectrode.

Note 2: The spectrum of the BSs, TiO_2, and $BiVO_4$ photoanodes in Figs. S14 and S15 were used to calculated the energy utilization of each component. For instance, in the hybrid system with BSs (Setup 3), the spectrum of BS1 - R represents the energy reaching the TiO_2 photoanode, the spectrum of BS1 - T + BS2 - R represents the energy reaching the $BiVO_4$ photoanode, and the spectrum of BS1 - T + BS2 - T represents the residual energy arriving at the PV cell. In the other two hybrid systems without spectral BSs, the spectrum of TiO_2 - T + $BiVO_4$ - T and TiO_2/$BiVO_4$ - T represent the energy arriving at the PV cell in the TiO_2 + $BiVO_4$ water splitting system and the TiO_2/$BiVO_4$ system, respectively. Meanwhile, the absorbance spectrum of TiO_2, $BiVO_4$ behind TiO_2, and TiO_2/$BiVO_4$ were shown in Figs. 8 and 10.

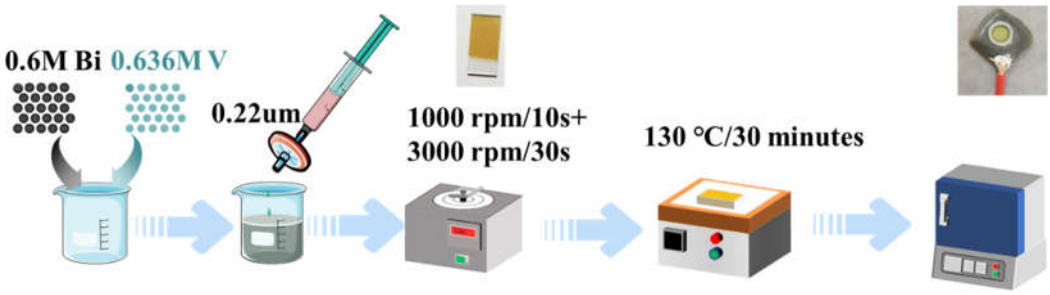

Fig. S1 Preparation of $BiVO_4$ photoanode.

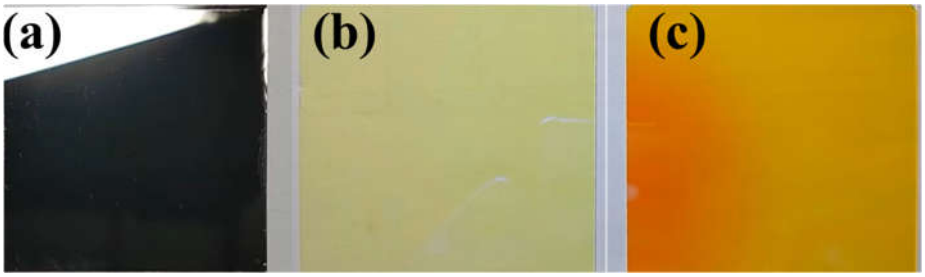

Fig. S2 Optical photos of BSs.

(a) Silver mirror; (b) BS1-BS reflecting 300–400 nm and transmitting 460–800nm; (c) BS2-BS reflecting 420–480 nm and transmitting 520–800 nm.

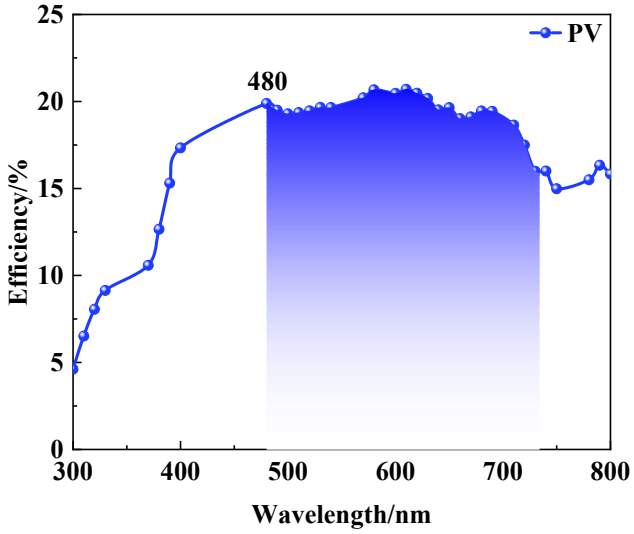

Fig. S3 Efficiency of the PV cell, from which more efficiency being found distributed in 480–800nm.

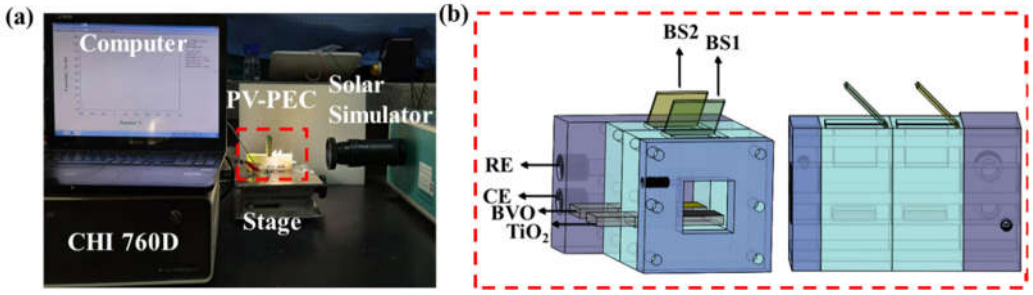

Fig. S4 System overview (photographs of the experimental novel hybrid PV-PEC system).

(a) Entire system during operation; (b) BS1, BS2, TiO_2 photoanode, $BiVO_4$ photoanode, Pt counter electrode, Ag/AgCl reference electrode.

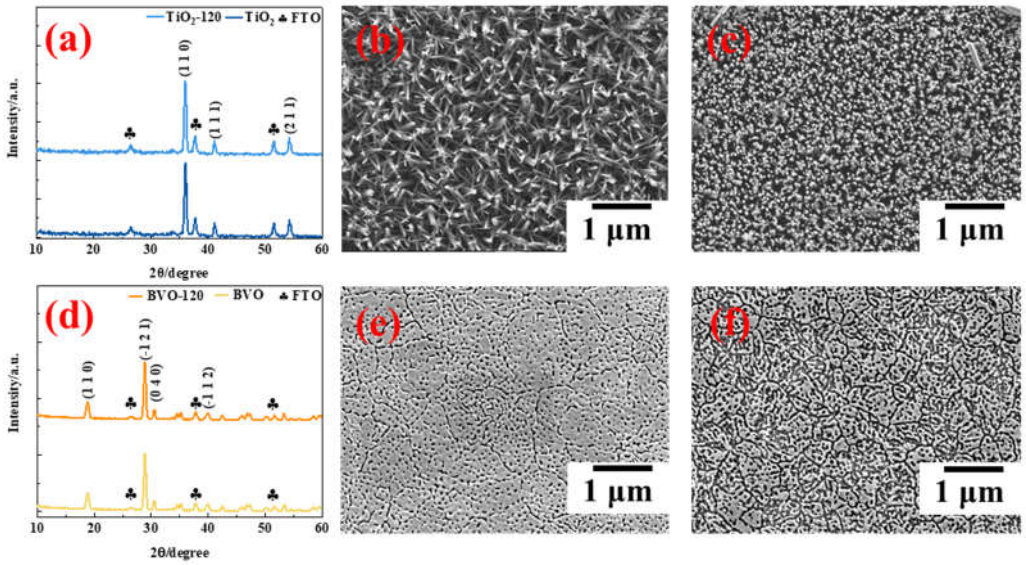

Fig. S5 XRD and SEM images of TiO_2 and $BiVO_4$ after irradiation for 150 minutes for water splitting.

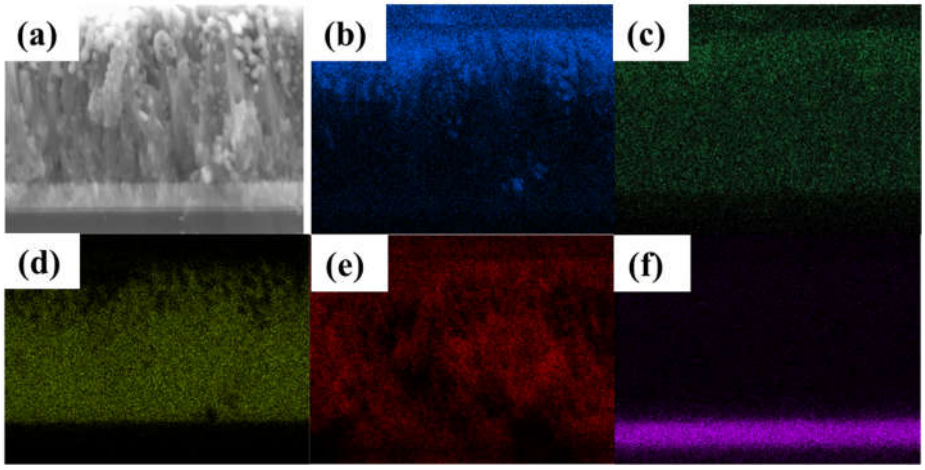

Fig S6 EDX elemental mapping of the $TiO_2/BiVO_4$ photoanode.

(a) SEM image; (b) Bi; (c) V; (d) Ti; (e) O; (f) Sn.

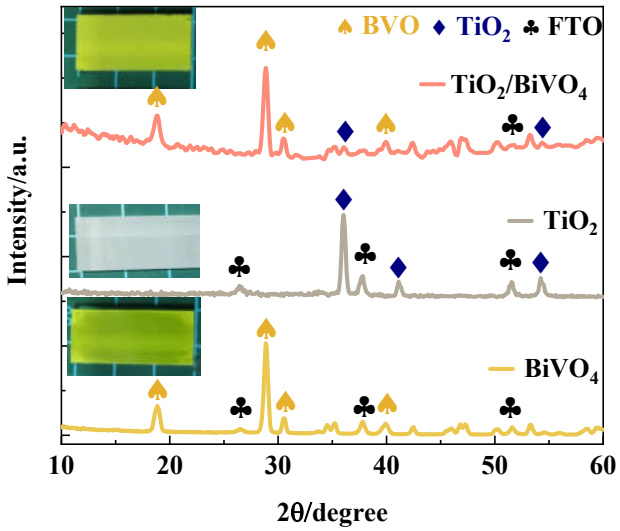

Fig. S7 Corresponding XRD patterns of $TiO_2/BiVO_4$ (the insert digital photos from top to bottom being $TiO_2/BiVO_4$, TiO_2, and $BiVO_4$, correspondingly).

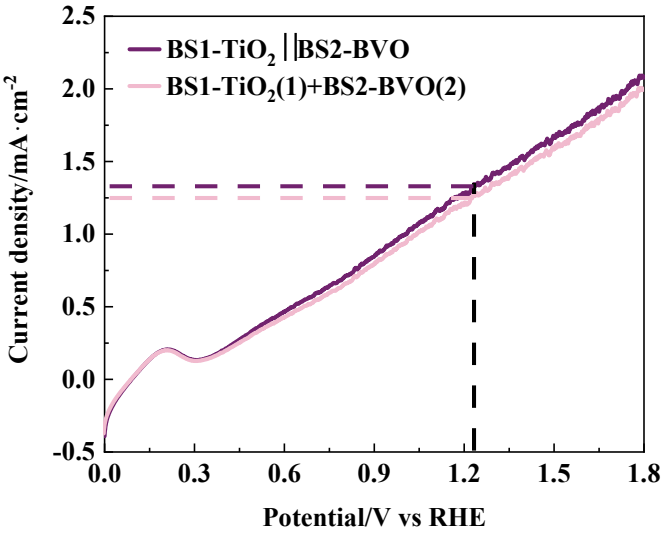

Fig. S8 Photocurrent density of TiO_2 and $BiVO_4$ photoanodes with BSs under a three - electrode system (TiO_2 - BS1|| $BiVO_4$ - BS2 representing the total current density of TiO_2 with BS1 and $BiVO_4$ with BS2, simultaneously; and TiO_2 - BS1 (1) + $BiVO_4$ - BS2 (2) representing the total current density of TiO_2 with BS1 and $BiVO_4$ with BS2, individually).

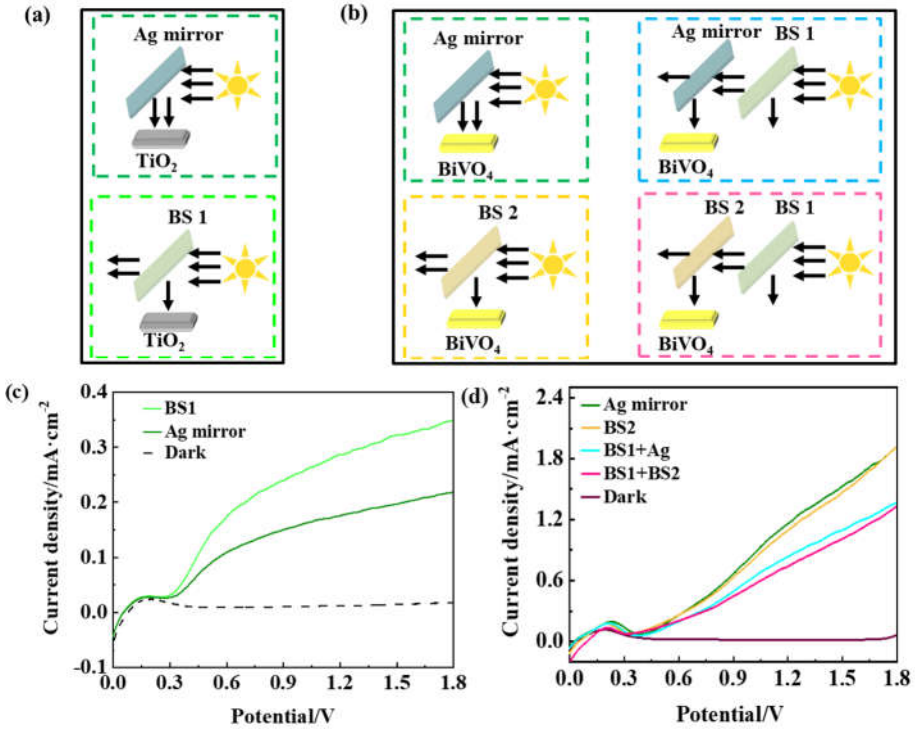

Fig. S9 Arrangement and photocurrent density.

(a,c) TiO_2; (b,d) $BiVO_4$ with different mirrors, respectively (the photocurrent density being obtained through a typical two-electrode system).

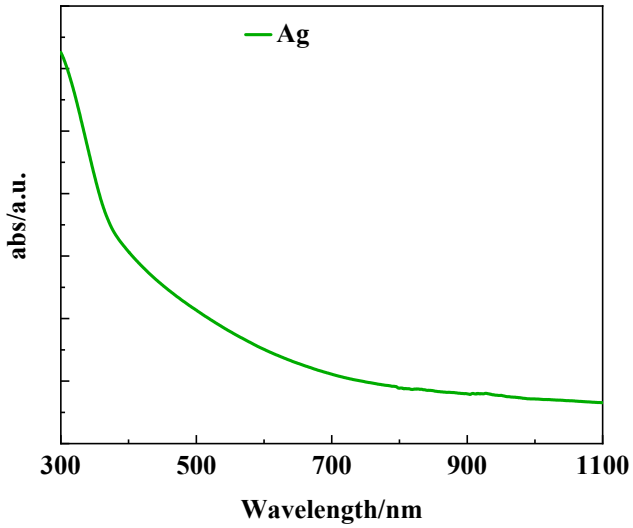

Fig. S10 Absorbance of Ag mirror between 300–1100 nm.

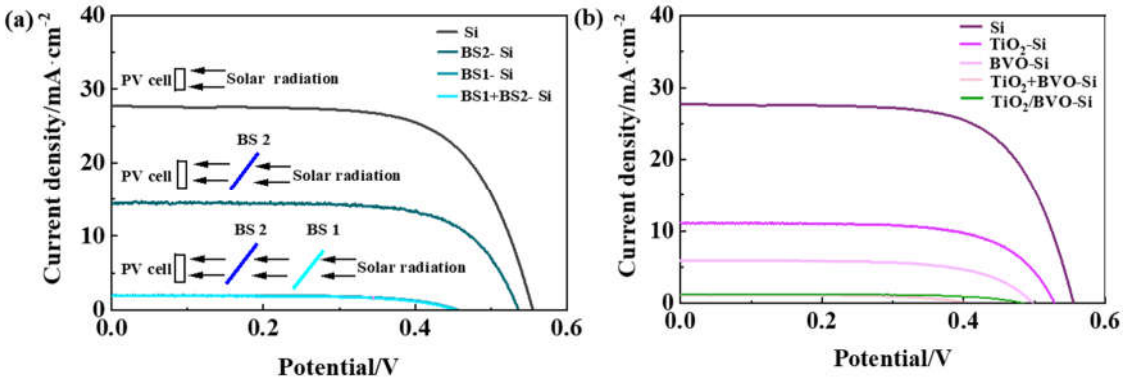

Fig. S11 PV electrical characteristics (current-voltage curves of Si cell under 1 sun illumination (AM 1.5 G, Xenon lamp)). (a) BSs; (b)$BiVO_4$, TiO_2, TiO_2+$BiVO_4$, and TiO_2/$BiVO_4$.

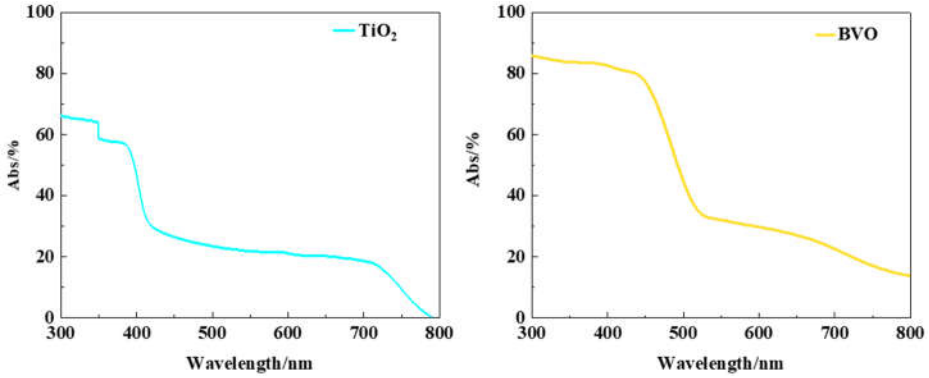

Fig. S12 Absorbance of TiO_2 and $BiVO_4$ photoanodes.

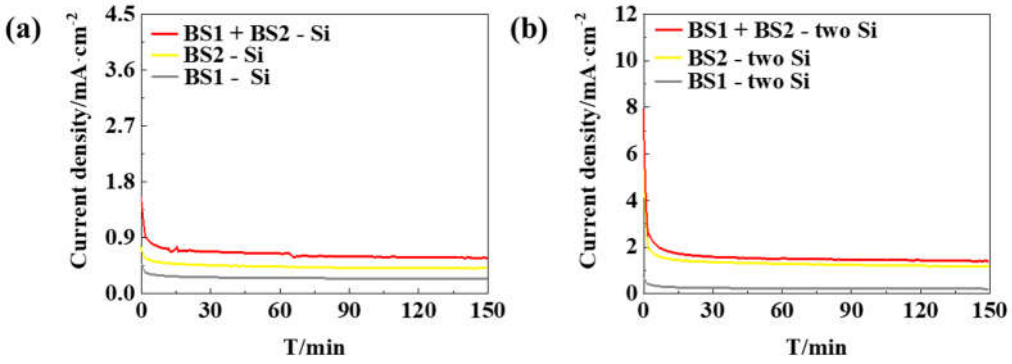

Fig. S13 *I*-t curves of the PV-PEC system based on BSs.

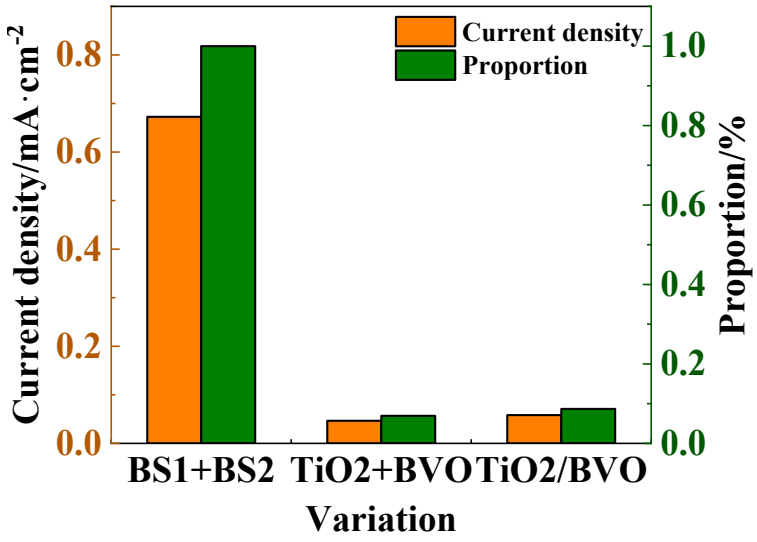

Fig. S14 Current density comparation and proportion of Setup 3 (BS1-TiO_2||BS2-BVO-PV), Setup 1(TiO_2+BVO-PV), and Setup 2 (TiO_2/BVO-PV).

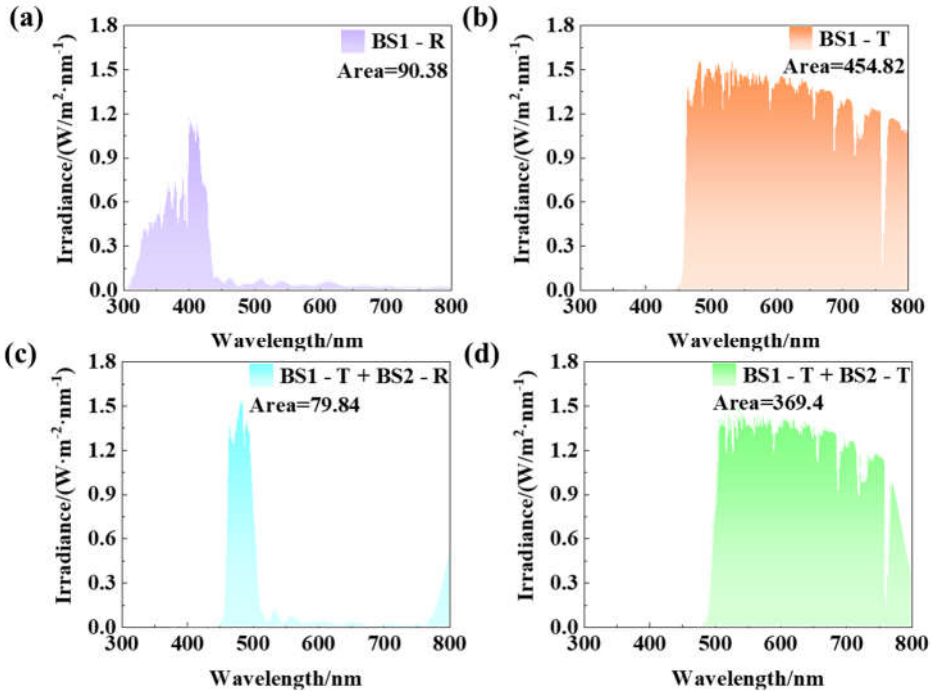

Fig. S15 Spectrum.

(a) Reflection of BS1; (b) transmittance of BS1; (c) reflection of BS2 after the transmittance of BS1; (d) transmittance of BS2 after the transmittance of BS1.

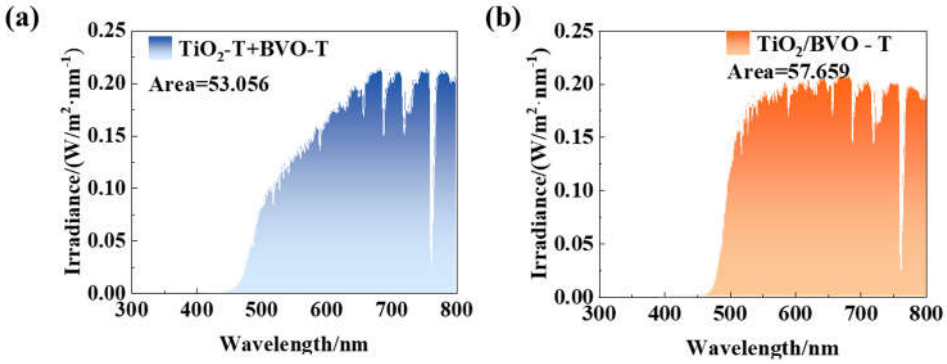

Fig. S16 Spectrum.

(a) Transmittance of TiO_2+$BiVO_4$; (b) transmittance of TiO_2/$BiVO_4$.

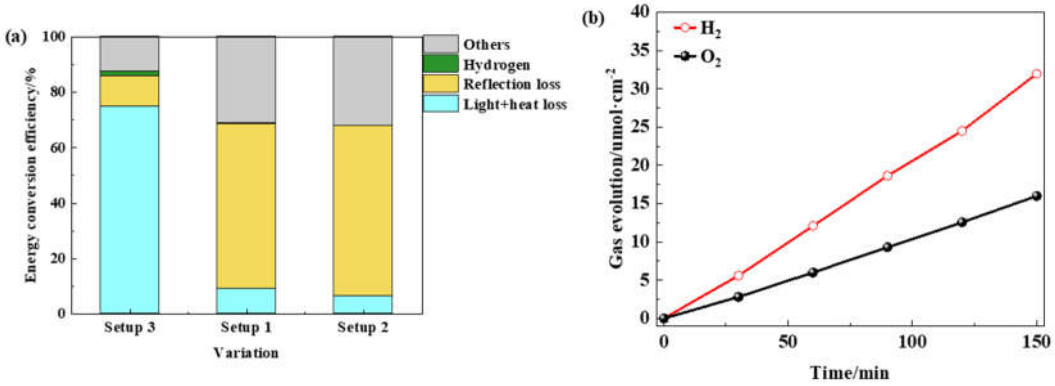

Fig. S17 Quantitative comparison.

(a) Spectrum usage with three different setups; (b) long-term gas evolution rates for H_2 and O_2 of Setup 3.

Table S1. System overview (an overview of selected system design parameters)

Description	Value
Amount of BS	2
Diameter of BS	1.5 cm ×1.5 cm
Angle of BS with light	45°
Distance of BSs	1 cm
Area of photoanodes	0.25 cm^2
Distance of photoanodes	1 cm
Diameter of PV	0.5 cm × 0.5 cm
Number of PV cells in system	1 or 2
PV type	monocrystalline silicon
Diameter of reactor	9.5 cm × 2.8 cm ×1 cm

Table S2. PV electrical characterization (results at 1sun with BSs (AM 1.5G))

Type	I_{SC}/mA	V_{OC}/V	I_{mpp}/mA	V_{mpp}/V	P_{mpp}/mW	FF/%	Efficiency/%
5×5 Si	6.5	0.56	5.37	0.44	2.36	64.8	9.4
BS1	0.5	0.46	0.41	0.36	0.15	65.2	0.6
BS2	3.61	0.54	3.22	0.42	1.35	69.3	5.4
BS1+BS2	0.47	0.45	0.40	0.35	0.14	66.2	0.56

Table S3. PV electrical characterization (results at 1sun with TiO_2+$BiVO_4$ structure (AM 1.5G))

Type	I_{SC}/mA	V_{OC}/V	I_{mpp}/mA	V_{mpp}/V	P_{mpp}/mW	FF/%	Efficiency/%
5×5 Si	6.5	0.56	5.37	0.44	2.36	64.8	9.4
Behind TiO_2	1.48	0.5	1.23	0.39	0.48	64.8	1.92
Behind $BiVO_4$	2.77	0.53	2.35	0.42	0.98	66.7	3.92
TiO_2+$BiVO_4$	0.28	0.40	0.24	0.29	0.069	61.6	0.28

Table S4. PV electrical characterization (results at 1sun with TiO_2/$BiVO_4$ structure at (AM 1.5G))

Type	I_{SC}/mA	V_{OC}/V	I_{mpp}/mA	V_{mpp}/V	P_{mpp}/mW	FF/%	Efficiency/%
5×5 Si	6.5	0.56	5.37	0.44	2.36	64.8	9.4
Behind TiO_2	1.48	0.5	1.23	0.39	0.48	64.8	1.92
Behind $BiVO_4$	2.77	0.53	2.35	0.42	0.98	66.7	3.92
TiO_2/$BiVO_4$	1.24	0.49	1.13	0.37	0.41	67.5	1.64

Table S5. Maximum power output of the single PV cell and the point of intersection under different type with BSs

Type	Maximum power point		Point of intersection	
	Voltage/V	Current density/mA·cm^{-2}	Voltage/V	Current density/mA·cm^{-2}
a	0.34	1.61	0.43	0.7
b	0.36	1.6	0.44	0.41
c	0.42	12.6	0.54	0.26

Table S6. Maximum power output of two PV cells in series and the point of intersection under different types with BSs

Type	Maximum power point		Point of intersection	
	Voltage/V	Current density/mA·cm^{-2}	Voltage/V	Current density/mA·cm^{-2}
d	0.72	2.71	0.9	1.54
e	0.76	4.15	0.97	1.16
f	0.86	7.13	1.07	0.31

Table S7. Maximum power output of and the point of intersection under different type with and without BSs for self-biased water splitting

Type	Maximum power point		Point of intersection	
	Voltage/V	Current density/mA·cm^{-2}	Voltage/V	Current density/mA·cm^{-2}
Setup 3	0.34	1.61	0.43	0.7

Setup 1	0.29	0.95	0.4	0.04
Setup 2	0.37	4.5	0.47	0.06

Table S8. Summary of recent representative reports on a tandem cell for water splitting under 1 sun illumination

No.	Photoanode	Photocathode	Electrolyte	STH (%)	Ref
1	FeOOH/NiOOH/BiVO$_4$||Ni$_2$FeO$_x$Fe$_2$O$_3$	PV:2 series-connected Si, CE: Pt	1.0 M KCi	7.7	[3]
2	BiVO$_4$/TiO$_2$/CoBi/TiO$_2$	BiVO4/TiO2/CoBi/TiO$_2$ PV: 2-jn a-Si, CE: Pt	1 M KBi	1.6	[4]
3	TiO$_2$||BiVO$_4$	TiO$_2$||BiVO$_4$ HIT-a-Si/n-c-Si/a-Si/ITO/TiO$_2$/Pt/	1 M KBi+0.2 M Na$_2$SO$_3$/1 M HClO$_4$	1.91	[5]
4	FeOOH/NiOOH/BiVO$_4$	Pt Coil	0.5 M potassium phosphate buffer	2.2	[6]
5	FeOOH/NiOOH/Fe$_2$O$_3$/BiVO$_4$	PV: tetra-cell Si solar cells, CE: Pt black	0.1 M sodium sulfate	3.2	[7]
6	dual-H, W:BiVO$_4$/CoPi PV:	PV: 2 series-connected SHJ, CE: Pt	0.1 M KPi	5.5	[8]
7	BS1-TiO$_2$||BS2-BVO-PV	PV: single Si,CE: Pt	0.5 M KBi	1.51	Setup 3
8	TiO$_2$+BVO-PV	PV: single Si,CE: Pt	0.5 M KBi	0.122	Setup 1
9	TiO$_2$/BVO-PV	PV: single Si,CE: Pt	0.5 M KBi	0.076	Setup 2

References

[1] S. Yang, B. Wang, R. Zhao, L. Wei, J. Su, Dalton Transactions 52 (2023) 16442–16450.

[2] N. Yang, S. Zhang, Y. Xiao, Y. Qi, Y. Bao, P. Xu, S. Jin, F. Zhang, N. Yang, S. Zhang, Y. Qi, Y. Bao, F. Zhang, S. Zhang, Y. Xiao, P. Xu, S. Jin, N. Yang, Angewandte Chemie International Edition 62 (2023) e202308729.

[3] J.H. Kim, J.W. Jang, Y.H. Jo, F.F. Abdi, Y.H. Lee, R. Van De Krol, J.S. Lee, Nature Communications 7 (2016).

[4] D. Xue, M. Kan, X. Qian, Y. Zhao, ACS Sustainable Chemistry and Engineering 6 (2018) 16228–16234.

[5] Z. Gong, B. Liu, P. Zhang, S. Wang, S. Jiang, T. Wang, J. Gong, ACS Materials Letters 3 (2021) 939–946.

[6] Y. Peng, G. V. Govindaraju, D.K. Lee, K.S. Choi, T.L. Andrew, ACS Applied Materials and Interfaces 9 (2017) 22449–22455.

[7] L. Li, J. Li, J. Bai, Q. Zeng, L. Xia, Y. Zhang, S. Chen, Q. Xu, B. Zhou, Nanoscale 10 (2018) 18378–18386.

[8] I.Y. Ahmet, Y. Ma, J.W. Jang, T. Henschel, B. Stannowski, T. Lopes, A. Vilanova, A. Mendes, F.F. Abdi, R. Van De Krol, Sustainable Energy & Fuels 3 (2019) 2366–2379.